A Mössbauer Spectroscopy Investigation of Nickel-Zinc Ferrites Synthesized by a Self-Combustion Method for Soft Magnetic Core Applications

Raphaël P. Hermann, George Yumnam, Kristyn D. Ardrey, and Beth L. Armstrong*

R. P. Hermann,[1] G. Yumnam,[1] K. D. Ardrey,[1] B. L. Armstrong[1]

1 Materials Science and Technology Division, Oak Ridge National Laboratory, Oak Ridge, TN 37831, USA

E-mail: hermannrp@ornl.gov

Keywords: ferrites, self-combustion, Mössbauer spectroscopy, magnetics

Soft ferrites are materials of interest for magnetic cores such as used for wireless charging transformers. Their low permeabilities, high resistivity and magnetic polarization make them interesting for high-power electric vehicle charging and drive systems. The nickel-zinc doped ferrites are of particular interest; however, the compositional space is quite large with respect to dopant concentrations, stoichiometric ratios and synthesis technique. Nickel-zinc spinel ferrites with varying nickel-zinc ratios prepared by a self-combustion reaction followed by heat treatment exhibit good crystallinity, and their low-temperature Mössbauer spectra show local magnetism and site occupation in agreement with materials prepared by solid state reaction. Thus, the combustion synthesis method offers a facile tuneability of compositions, which, combined with the possibility of rapid characterization of atomic-scale magnetism by Mössbauer spectroscopy, enables advances in the compositional and processing space at a fast pace. In the low-temperature Mössbauer spectroscopy data for samples with increasing nickel content, there is a systematic increase in average hyperfine field (2.8 T/Ni) and decrease in average isomer shift (-0.036 mm/s/Ni) that can be utilized for assessing the nickel/zinc content, even in the absence of applied magnetic field data. A gradual evolution of color is also observed with increasing nickel content, albeit trends in color depend on sintering conditions.

1. Introduction

Ferrites are technologically important materials in many modern electronics applications. They are used as cores in high-frequency transformers, as antennas,[1] and in various high-frequency circuits, where they act as filters or electromagnetic interference inhibitors.[2,3] They have also found use for magnetic recording, magnetic resonance imaging, and as sensors in the

automotive industry.[4-6] Their use as soft magnetic core for transformers is now finding a new application in systems that enable wireless transmission of large amounts of power, notably for the electric vehicle industry.[7] Their high resistivity and magnetic polarization enable operation at higher frequency than metallic cores.[8]

Among ferrites, the AB_2O_4 spinel ferrites, with *A* and *B* divalent and trivalent cations, respectively, are isostructural to and derived from Fe_3O_4 magnetite, one of the oldest known magnetic materials.[9] The *A* and *B* site cations are tetrahedrally and octahedrally coordinated, see **Figure 1**. The spinel structure-material adopt the $Fd\bar{3}m$ space group (227), bearing 8 *A*-site cations, 16 *B*-site cations, and 32 oxygen ions in the conventional unit-cell (a~ 8.4 Å, V~ 600 Å^3).[10,11] There is a large flexibility in the cations that can be accommodated in the spinel structure and countless solid solutions have been investigated, notably by means of Mössbauer spectroscopy.[12,13] Mössbauer spectroscopy was instrumental in revealing the correlated change in magnetic and charge properties in magnetite, *i.e.* the Verwey transition,[14] and remains crucial for investigating the magnetic properties and site occupation in spinel ferrites and nanoferrites. When magnetic, the spin of the cations on the *A* site is antiparallel to the spin of the *B*-site cations. Hence, the materials are ferrimagnetic.[15] The spins are however not always strictly antiparallel and several studies using for example Mössbauer spectroscopy or neutron diffraction have focused on spin-canting.[16,17]

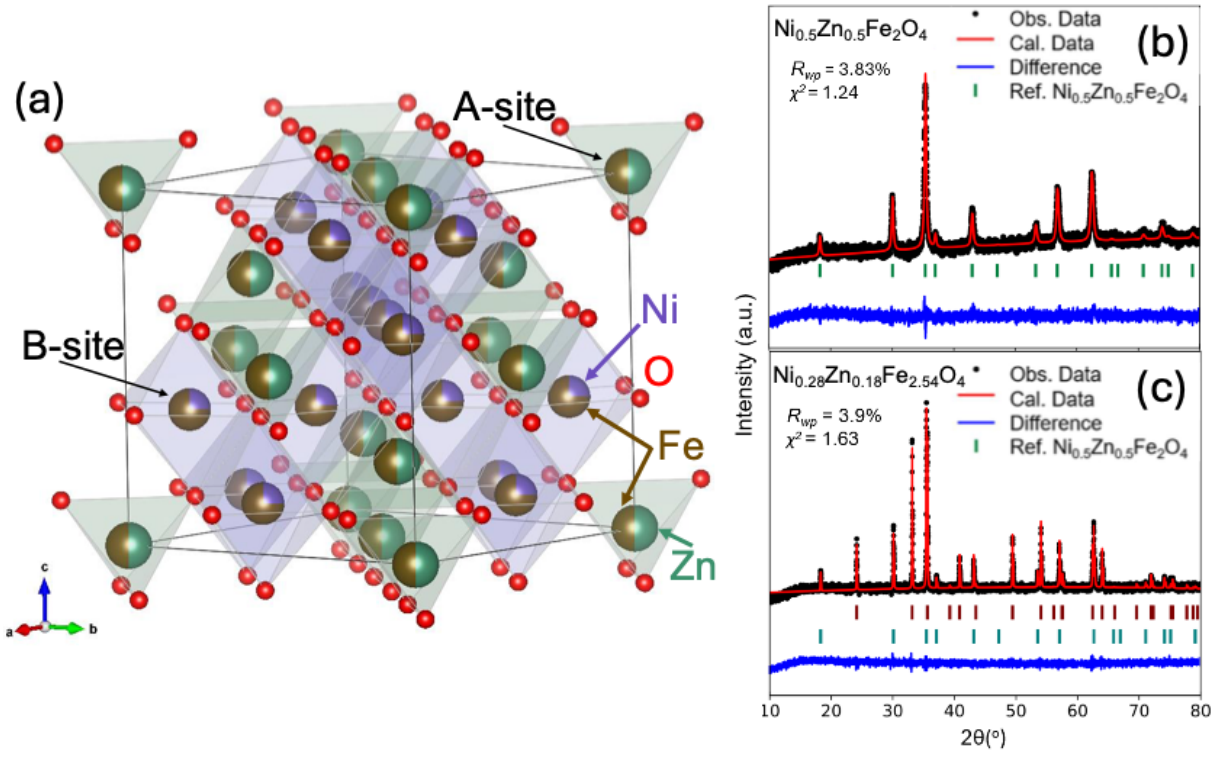

Figure 1. Spinel structure (left) of the $Ni_{1-x}Zn_xFe_2O_4$ ferrites and X-ray diffraction patterns with Rietveld analysis (right) of two selected materials, see text. The presented structure is derived from ICSD[18] collection code 96663[19] for $Ni_{0.5}Zn_{0.5}Fe_2O_4$ with Zn and Ni exclusively on the *A* and *B* site, respectively, drawn using VESTA.[20]

For wireless charging applications, two spinel ferrite solid solutions are of particular interest, both due to their magnetic properties and due to the absence of critical elements. $(Zn,Mn)Fe_2O_4$ and $(Zn,Ni)Fe_2O_4$ exhibit large relative permeabilities (μ_r ~ 4500 and ~ 2300, respectively) and saturation magnetization (M_S ~ 60 and ~ 50 emu/g, respectively);[21-23] both exhibit a composition dependent Curie temperatures, which can be tuned to above 200°C – sufficiently high for applications – by moving away from the $ZnFe_2O_4$ end-member, which is paramagnetic in the bulk-phase. Although these materials have intended use for wireless charging applications, their dynamic magnetic susceptibility will not be reported here. The purpose of this study is rather to assess the impact of the Ni/Zn ratio on atomic scale magnetism and whether the materials synthesized by this solution combustion method exhibit similar properties to those reported earlier. Here, we will focus on the $(Zn_{1-x}Ni_x)Fe_2O_4$ system, with $0.2 \leq x \leq 0.9$. The end members of the solid solution are $ZnFe_2O_4$, a normal spinel, *i.e.* featuring no trivalent iron on the *A* site, and $NiFe_2O_4$, an inverse spinel with Ni occupying the *B* site and trivalent iron on the *A* site.[12]

The synthesis method and cost associated with precursors, synthesis temperature, and heat treatment bears critical importance for application at large scale. Spinel ferrites have been prepared by several methods, [24] notably polyol method,[25] sol gel,[26] coprecipitation,[27] solid state,[13,28] and the combustion method, *e.g.* using citric acid and formation of a xerogel.[29-32] Here, we study $(Zn_{1-x}Ni_x)Fe_{2-\beta}O_{4-\alpha}$ synthesized by the self-combustion method of precursor nitrates, a method that offers facile composition tunability by simple mixing of liquid precursors. For stoichiometric materials, α and β, which mark deviation of oxygen content and iron content from the nominal spinel composition, are both 0. The materials we discuss are generally stoichiometric, and results for two off-stoichiometric material, with $\beta \neq 0$ and $\alpha \neq 0$, are shown only for illustration. The materials have been characterized by X-ray diffraction (XRD), X-ray fluorescence (XRF), colorimetry and by iron-57 Mössbauer spectroscopy at room temperature and 6.5 K. These methods reveal that the synthesis method yields high quality, well crystallized materials, with site occupation and hyperfine fields compatible with those observed in material synthesized by high-temperature powder reaction.[13]

2. Methods

Synthesis: The samples were commercial powder of (Zn,Ni)Fe_2O_4 spinels prepared using a solution combustion synthesis reactor at Steward Advanced Materials. The precursors were iron nitrate, nickel nitrate, and zinc nitrate in aqueous solution, mixed to desired stoichiometric ratios. The starting solutions were all 99 to 99.5% pure. Gravimetric analysis was used to standardize the nitrate solutions, which were weighed out during preparation. The solutions were homogenized for 30 minutes to 1 hour before a proprietary fuel was added and the solution was homogenized for an additional hour. The solutions were sprayed in a continuous reactor at 350°C to form the raw powder. The synthesized powder was further calcined at 600°C for 30 minutes to remove any residual carbon or unreacted fuel, before further heat treatment indicated in Table 1. The heat treatment temperatures for all the samples evaluated, except those with x=0.5 (equal Ni/Zn dopant ratios) were based on temperatures required to achieve 100% conversion to the spinel phase. The increased temperature between the x=0.8 and x=0.9 also reflects the dopant dependence for full conversion to spinel phase. The lower/shorter calcination temperatures of the x=0.5 samples B and C were intentional, to study if there was an impact of this condition on the crystallinity and atomic scale magnetism.

X-ray diffraction: The ferrite powders were analyzed by X-ray diffraction (XRD), using a Rigaku SmartLab diffractometer with a Cu-K_α (λ=1.5406 Å) source with a voltage of 40 kV and current of 38 mA. Scans were taken in a 2θ range of 10-80° with a 0.01° step size at a speed of 5°/min. Total data points per scan equaled to 7001. Phases identified via XRD were analyzed by Rietveld refinement utilizing GSAS II software[33] with crystallographic references sourced from the Inorganic Crystal Structure Database (ICSD)[34].

X-ray fluorescence: XRF analysis was carried out on 5 g samples using a PANalytical Epsilon 4 system with a silver anode with a Be encapsulated window on loose powder. The data was analyzed using the PANalytical XRF with the Omnian software. This approach does not use a standard but has built in calibration curves as a reference and only includes elements that have been detected and determined to be significant.

Mössbauer spectroscopy: Iron-57 Mössbauer spectra were acquired at room temperature and at the base temperature of the Janis SHI-800 close-cycle cryostat, ~6.5 K. Spectra were obtained in zero applied magnetic field. Power samples with ~45 mg/cm^2 were mixed with boron nitride; all samples had natural isotopic abundance. A krypton gas proportional counter, registering the

14.4 keV and the Kr-escape peak, and a Tl@NaI proportional counter (Ritverc GmbH) were utilized for room temperature at low temperature, respectively. The velocity transducers (Wissel GmbH) were calibrated using α-iron foil, which also serves as isomer shift reference. The radiation source was ^{57}Co in rhodium matrix with ~ 5 mCi activity.

To analyze the spectra, the fitting method below was used, because resolving the *A* and *B* site occupation for Fe is unreliable in the absence of data acquired in applied magnetic field. Thus, data was fitted by using the nominal Fe site occupations obtained when assuming that Ni and Zn can only occupy the octahedral *B* site and tetrahedral *A* site, respectively[13]. Considering only stoichiometric compounds (α,β=0) the relative areas for the sextet ascribed to Fe on the *A*-site and *B*-site is *x* and 2-*x*, respectively, whereas the ratio of *A*-site over *B*-site area is *x*/(2-*x*). For off-stoichiometric materials, hematite, α-Fe_2O_3, was identified as secondary phase and its parameters were added to the fit model. Further free fit parameters are the isomer shift, δ, quadrupole splitting, ΔE_Q, hyperfine field, H_{hf}, and linewidth, Γ, for the *A* and *B* site. We also constrained the relative areas of the six sextet lines to the 3:2:1:1:2:3 ratio usual for powders, because preliminary fits indicated (as expected for a cubic material) no magnetic preferential orientation that would modify the intensity of the lines 2 and 5 lines. A single incremental linewidth parameter each was used to mimic hyperfine field distribution for the A and B site; accordingly the line widths vary as $\Gamma = \Gamma_0 * v.IW$, with *v* the velocity and IW the incremental linewidth. Fit values obtained by Leung et al. were used as starting point for the fits.[13]

Macro-photography and colorimetry of ferrite specimens: Each ferrite sample was prepared by uniaxial pressing of dry powders into 10 mm diameter disks. Samples were photographed on white paper background with flash photography with the camera held at 15 cm from the sample surface. Brightness of the photographs was adjusted to the exact same level for each sample to ensure good visibility on printed paper. Colorimetry for the powders was also carried out using a NIX Spectro 2 spectrophotometer. Powder was placed into a plastic cup until full and level with the top, so the measurement surface was level and uniform. An internal calibration was performed to eliminate white noise prior to each set of three measurements. The lens of the spectrophotometer was placed onto the powder and 3 measurements are taken. A total of nine measurements were taken of each sample. The results are reported in Table 1 following the CIE *L*a*b** standard[35], where *L** codes the lightness between 0 and 100 (black to white), *a** codes the green/red axis (negative to positive) and *b** codes the blue-yellow axis negative to positive).

3. Results

The ferrite powders with heat-treatment conditions listed in **Table 1** were characterized by X-ray diffraction, and two patterns are shown in Figure 1 for $Ni_{0.5}Zn_{0.5}Fe_2O_4$ (sample A) and the off-stoichiometric material $Ni_{0.28}Zn_{0.18}Fe_{2.54}O_4$. All data were analyzed by pattern matching and the latter two were analyzed by Rietveld refinement. The $Ni_{0.5}Zn_{0.5}Fe_2O_4$ powder was found phase pure cubic ($Fd\bar{3}m$) with a residual weight of R_{wp} = 3.8%. In contrast the $Ni_{0.28}Zn_{0.18}Fe_{2.54}O_4$ powder was found to be dual phase, with both a spinel cubic phase (47 wt.%; a=8.379 Å) trigonal hematite phase Fe_2O_3 ($R\bar{3}c$; *a=5.03 Å;c=13.74 Å*) (53 wt.%) with a weighted residual of R_{wp} = 3.9%. Rietveld refinements were conducted utilizing crystallographic references, Fe_2O_3 (PDF-01-088-3889)[3] and $Ni_{0.5}Zn_{0.5}Fe_2O_4$ (PDF-01-090-3511).[4] Some reflections that are not visible in the patterns are minor reflections and their absence is attributed to being lost within the background noise.

Table 1. Composition, heat-treatment, lattice constant, and colorimetry data of stoichiometric $Ni_xZn_{1-x}Fe_2O_4$ samples. The error bar on the lattice constant is 0.0005 Å.

x in $Ni_xZn_{1-x}Fe_2O_4$	Heat treatment		Lattice constant	Colorimetry		
	Temperature [ºC]	Time [hours]	[Å]	*L**	*a**	*b**
0.2	1100	5	8.4336	29.8	12.7	6.12
0.4	1100	5	8.4246	29.4	10.6	3.92
0.5 Sample A	900	4	8.3955	35.1	16	14.6
0.5 Sample B	600	1	8.3961	26.2	11.4	7.72
0.5 Sample C	600	0.5	8.3995	35.7	14.1	11.6
0.6	1100	5	8.4049	28.4	6.64	0.61
0.8	1100	5	8.3630	29.5	5.38	-0.3
0.9	1300	1	8.3481	28.9	5.08	-0.6

The lattice constants extracted from X-ray diffraction data decrease with increasing nickel content, see **Figure 2**. This general trend agrees with that observed by Leung et al.,[13] with some deviation for the *x*=0.4 and *x*=0.6 material. XRF was used to analyze the stoichiometric ratios of the *x*=0.4, *x*=0.5. and *x*=0.6 materials to determine if compositional variation could explain the deviation in the lattice constants in this range. The data, shown in **Table 2**, compares the measured (actual) Fe, Zn, and Ni molar concentrations versus the nominal, batched or calculated, concentrations used during the synthesis process. The actual composition is consistent with the nominal concentrations and within standard deviation of the measurement

technique. The lattice constant variation for the x=0.4 and x=0.6 is not a result of off–stoichiometric composition and has yet to be explained. Note also, see Table 1, that for x=0.5 material, three samples with same composition were prepared. These samples differ by the heat treatment. The lattice constant decreases with increasing heat-treatment (time and temperature), presumably as strain is released in the material.

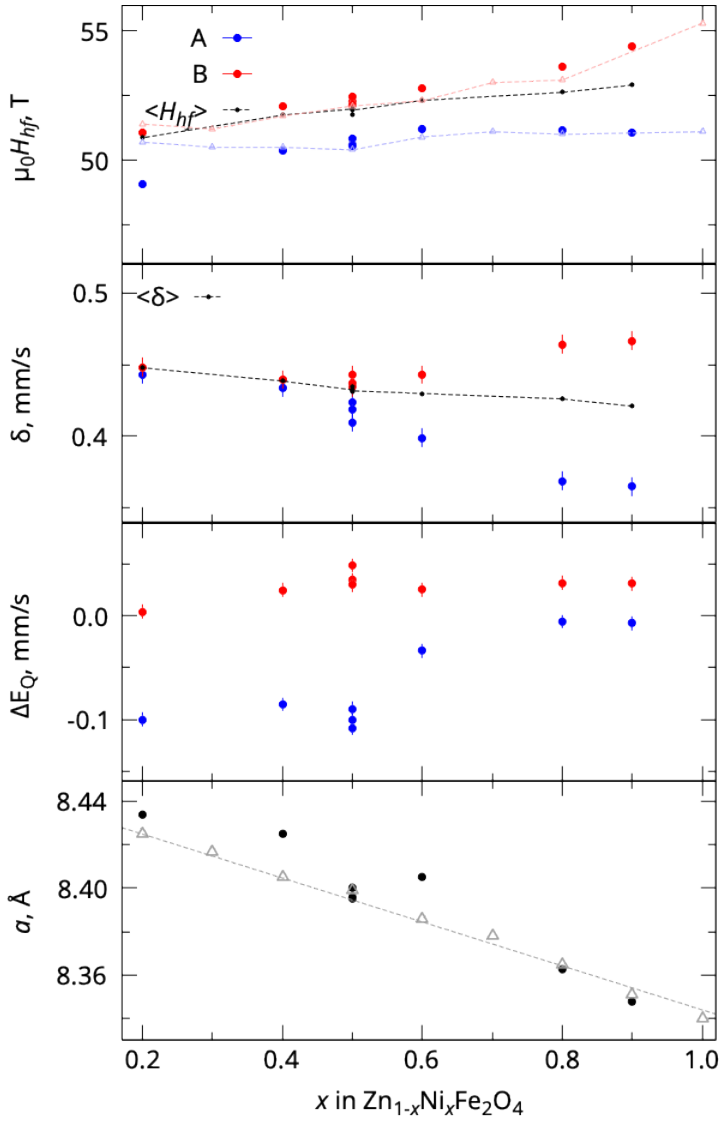

Figure 2. Lattice constant *a* obtained from X-ray diffraction and Mössbauer spectral parameters obtained from fits of the 6.5 K data, as a function of the Ni content, x, in $(Zn_{1-x}Ni_x)Fe_2O_4$. Filled circles: this study; A-site in blue, B-site in red; relative areas are fixed to $x/(2-x)$ for A/B. The black dashed line indicates the occupation-weighted average hyperfine field and isomer shift. For the lattice constant, open triangles: Leung *et al.*[13], light dashed lines: guide to the eye.

The increase in nickel content is accompanied with a gradual change in color of the material, as shown in **Figure 3**. Whereas the materials closer to $ZnFe_2O_4$ are light brown, materials closer

to $NiFe_2O_4$ takes a darker grey, slightly purple, shade. However, note that the trends are only qualitative and that there is significant variation related to heat treatments.

Table 2. Composition, in atomic percent, for select materials, actual, as determined by X-ray fluorescence, and nominal. The typical error bar is 0.05%.

Composition		Fe [%]	Zn [%]	Ni [%]	Total [%]
$Ni_{0.6}Zn_{0.4}Fe_2O_4$	Actual	67.54	13.18	19.09	99.81
	Nominal	66.66	13.30	20.00	99.99
$Ni_{0.5}Zn_{0.5}Fe_2O_4$	Actual	66.737	16.28	16.81	99.83
	Nominal	66.66	16.66	16.66	99.98
$Ni_{0.4}Zn_{0.6}Fe_2O_4$	Actual	66.87	19.88	12.83	99.58
	Nominal	66.66	20.00	13.33	99.99

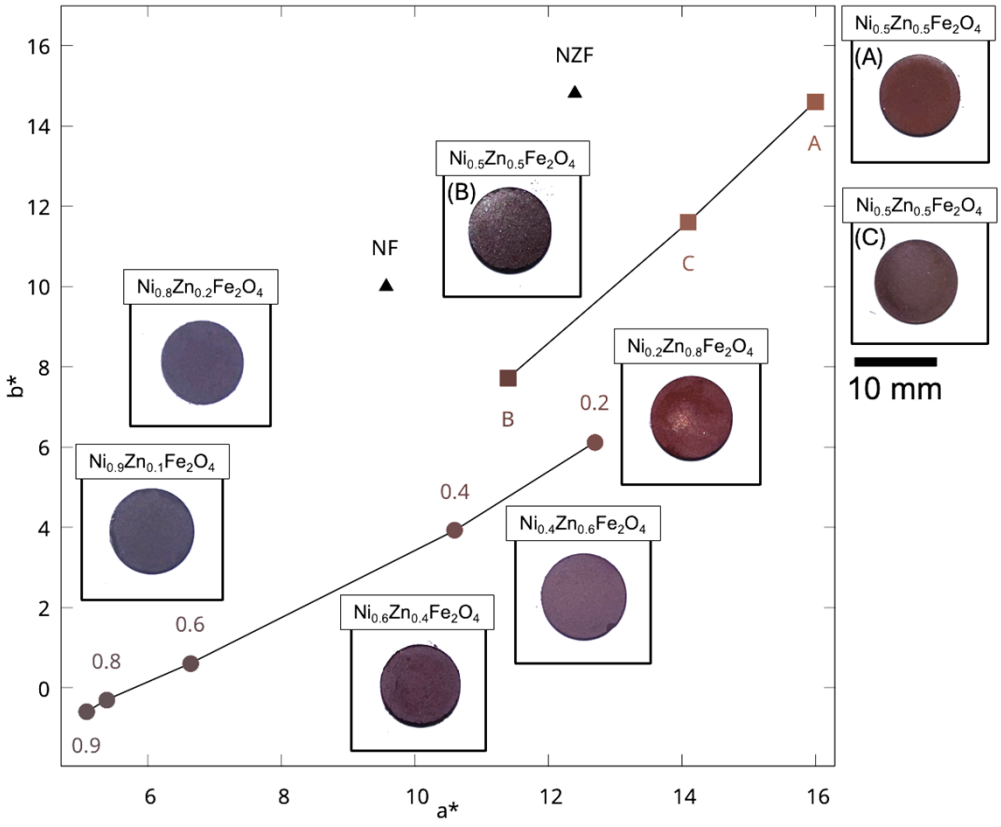

Figure 3. L*a*b* colorimetric data for powders of spinel ferrites. The number next to circles in the Ni content; A, B, C denote the samples with $Ni_{0.5}Zn_{0.5}Fe_2O_4$, see Table 1; black triangles

denote $NiFe_2O_4$ (NF) and $Ni_{0.5}Zn_{0.5}Fe_2O_4$ (NZF) in Ref. [36]. Macro photographs of pressed, unsintered, pellets of the spinel ferrite series are placed near corresponding data points.

The Mössbauer spectra obtained at room temperature, see **Figure 4**, bear witness to the gradual decrease in magnetic ordering temperature with decreasing nickel content. The magnetic hyperfine splitting gradually decreases as x decreases and vanishes for x=0.2, indicating that this material is paramagnetic (or superparamagnetic) at room temperature, in agreement with T_C~250 K reported by Leung *et al.*[13] Note that for the materials with the highest ordering temperature, x=0.8 and 0.9, there is a clear signature of two discrete hyperfine fields, associated to the *A* and *B* site, see blue and red lines at the top of Figure 4, best seen in the outer spectral lines at positive velocity. This splitting vanishes and gets washed out with decreasing x, as the spectra broaden significantly due to a distribution of hyperfine fields –presumably caused by a distribution in grain size and Curie temperature. Based on the fits obtained at low temperature, see below, we have attempted to mimic the spectral shape at room temperature with a magnetic relaxation model aiming at capturing the potential superparamagnetic behavior. This model did not yield a satisfactory qualitative description of the spectra. Comparison with the spectral shape observed in superparamagnetic maghemite (γ-Fe_2O_3)[37] and nanosized nickel-zinc ferrites[38] also suggests that the materials are too coarse grained to exhibit superparamagnetic behavior. This is also in agreement with grain sizes larger than 100 nm expected from the absence of Debye-Scherrer broadening in the X-ray diffraction pattern. We have not carried out further attempts to fit the room temperature spectra, because the extracted information would be less reliable than for the low-temperature spectra. The room temperature spectral shapes indicate that instead of superparamagnetic relaxation, a grain-size- and possibly local-composition-dependent distribution ordering of temperatures, and thus of hyperfine fields, leads to the broadened spectra. For the $Ni_{0.5}Zn_{0.5}Fe_2O_4$ phase, materials B and C with the lower calcination temperature exhibit some residual paramagnetic phase, ~10% at., visible in the center of the spectrum. Thus, the higher calcination temperature is needed to promote transformation of the entire material to a ferrimagnetic phase.

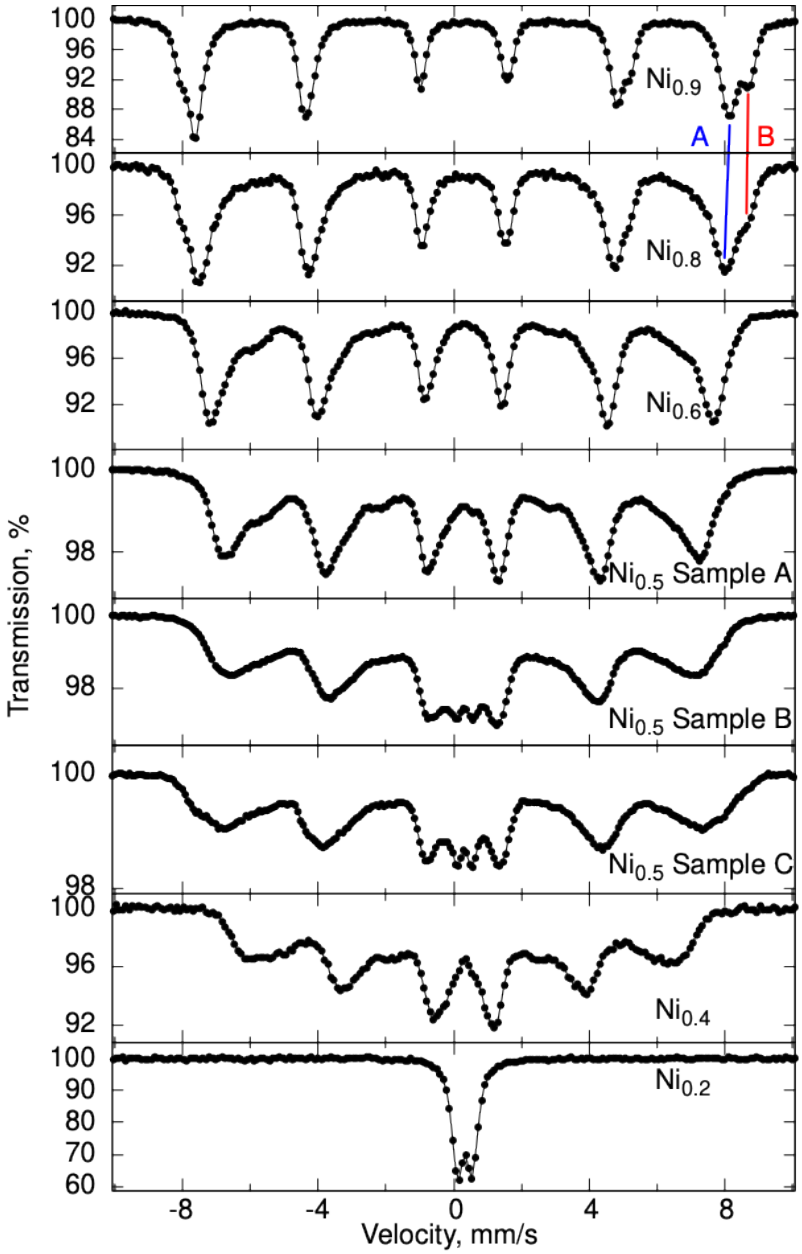

Figure 4. Room temperature Mössbauer spectra of $(Zn_{1-x}Ni_x)Fe_2O_4$. The blue and red line in the top two spectra indicates the position of the outer line of the A- and B-site sexted, respectively.

The Mössbauer spectra at low temperature for the stoichiometric material all exhibit, see **Figure 5**, a very clean magnetic hyperfine split sextet, with fairly narrow lines (width ~0.36 mm/s for the fits in Figure 5; except 0.44 mm/s for x=0.9). There is however gradual broadening and eventual splitting of the outermost line at positive velocity with increasing x, which reflects the gradual increase of the *B*-site hyperfine field with increasing nickel content.[13] The spectra could readily be fitted with a two-site model (A-site and B-site are shown as blue and red curve, respectively), see Methods, and the extracted hyperfine parameters are shown in Figure 2. Except for possibly the x=0.8 and 0.9 spectrum, the resolution is not sufficient to unambiguously differentiate the *A* and *B* site hyperfine field and occupation at the same time, in the absence of an applied magnetic field.[13,26,27,39] Hence, we utilized the site occupation derived from the assumption of exclusive *A*-site occupation for Zn and *B*-site occupation for Ni. With the utilized model, satisfactory fits are obtained, and the composition dependent spectral parameters are in good agreement with those determined by Leung et al. .[13] However, note that the hyperfine field that we observe for the *B* site is slightly larger than in their report, possibly due to a different approach to line-broadening fitting, and that the isomer shift exhibits a substantially clearer systematic trend. We hope to resolve these issues in a future study when an applied magnetic field system becomes available and will help resolve more details without overfitting. The quadrupole splitting values are also qualitatively in agreement but might warrant more detailed investigation. For two spectra, it was necessary to fix the quadrupole splitting for the *A* site to -0.1 mm/s, due to anti-correlation with the *B*-site value. Note that the present data has substantially better statistics than in Leung et al.,[13] and small weaknesses in the simple fit model used here are more readily visible. The hyperfine field is mostly constant for the *A* site, close to ~50.6 T, and gradually increases with Ni content for the *B* site, where a field of 54.8 T, *e.g.* similar to values observed by Chappert *et al.*[40] . Overall, we observe a robust trend in average hyperfine field and isomer shift with increasing Nickel content, where the slope are +2.8 T and -0.036 mm/s per nickel, respectively. These trends can be utilized to assess Ni/Zn ratios, without requiring applied magnetic field data.

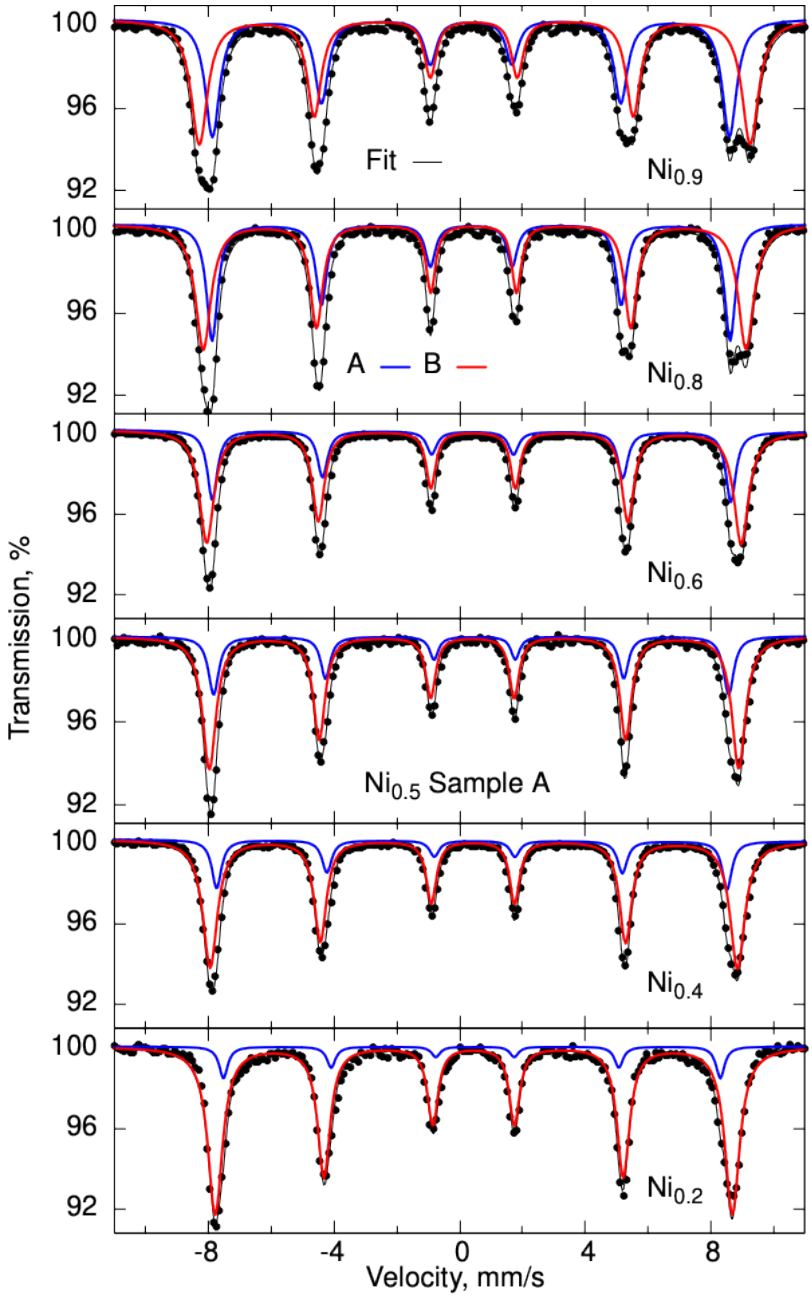

Figure 5. Mössbauer spectra of $(Zn_{1-x}Ni_x)Fe_2O_4$ labeled by their Ni content measured at 6. 5 K. Subspectra and total fit are shown with a blue (A-site), red (B-site) and black line (total fit).

The low-temperature spectra for the two off-stoichiometric materials, and the materials with x=0.5 with different heat-treatment are shown in **Figure 6**. For the off-stoichiometric materials, the presence of a hematite impurity phase is readily visible, as also indicated by X-ray diffraction. By using a preliminary fit with hematite and a single sextet for the ferrite, we have determined the average hyperfine field of the ferrite phase (supposing a composition of $Ni_xZn_{1-x}Fe_2O_4$), which was then used with the data in Figure 2 to determine a best guess for the value of x in the phase. The final fits that are shown utilize constrained spectral parameters with only the relative amount of hematite and the linewidths as fit parameters. The ratio of A/B

determined for the spinel part of the spectra, after subtraction of the hematite, based on the average hyperfine fields of 51.9 and 52.5 T, was ~0.30 and ~0.38, corresponding to a composition of $Ni_{0.46}Zn_{0.54}Fe_2O_4$ and $Ni_{0.55}Zn_{0.45}Fe_2O_4$ for the samples "$Ni_{0.28}Zn_{0.18}$" and the "$O_{3.6}$", respectively. Comparing with the nominal stoichiometries indicates that some nickel and/or zinc are accommodate in the hematite phase, as in Ref. [41].

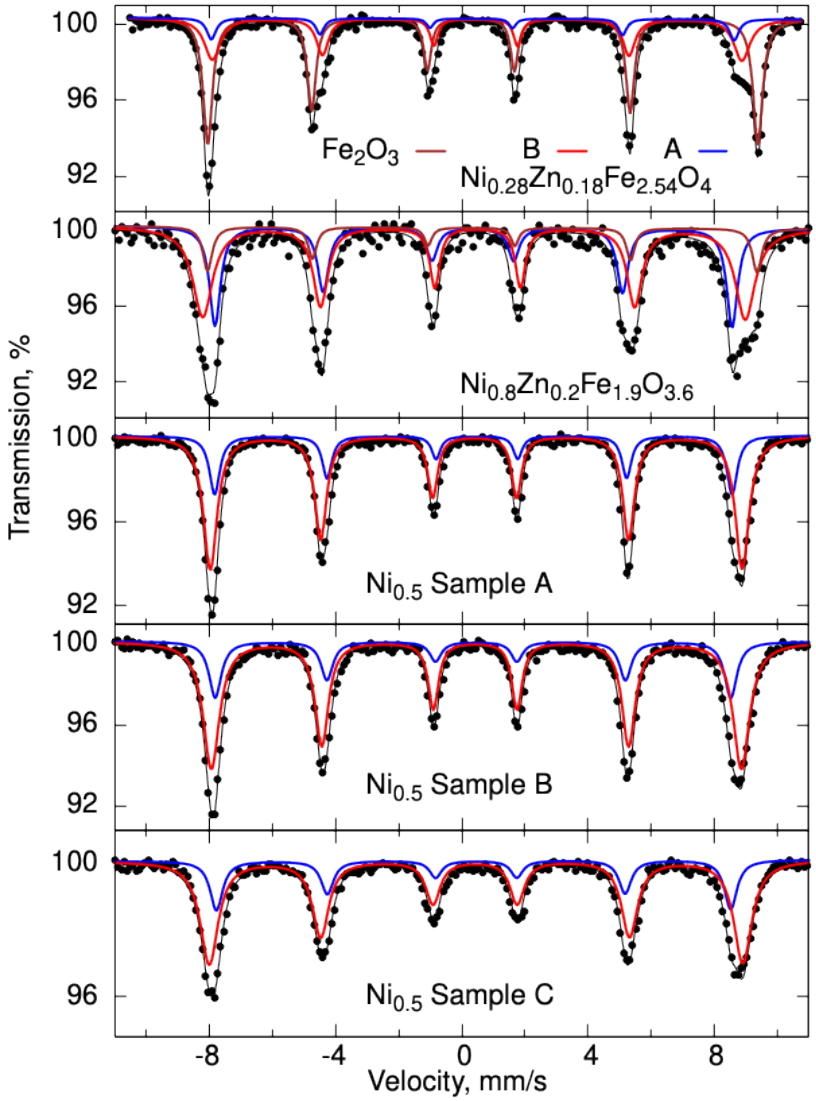

Figure 6. Low-temperature spectra of off-stoichiometric materials and the $Zn_{0.5}Ni_{0.5}Fe_2O_4$ material, with different heat treatment (Sample A: 900ºC/4 h–same data as in Figure 4, Sample B: 600ºC/1 h, Sample C: 600ºC/30 min.). Subspectra and total fit are shown with a blue (A-site), red (B-site), brown (Fe_2O_3) line, and black line (total fit).

For the x=0.5 materials, the spectra reveal that increasing heat-treatment (time and temperature) leads to more narrow lines associated to better material crystallinity. Interestingly though, the

least annealed material exhibits a slightly larger hyperfine field, presumably caused by local variation in the *x*-value that get resolved after annealing.

4. Discussion

The primary goal of this study was to assess the quality of the powders generated by a solution self-combustion method and moderate heat treatment. This study indeed confirms that this yields high quality, well-crystallized materials, with site occupations compatible with those observed in material synthesized by high-temperature powder reactions.[13] This solution combustion approach to synthesize $(Zn,Ni)Fe_2O_4$ spinels also allows variation in the Zn/Ni ratio. Crystallinity can be tuned using variable heat treatment temperature and duration. Classically, these powders are annealed to grow the particle/grain size to maximize magnetic properties in the starting powder and until the composition is single phase. Because larger particle sizes will decrease the densification rate during the subsequent sintering process, the variation in annealing temperature and time in the x=0.5 compositions were used to assess control of sintering temperatures and times *in-situ*. A remaining paramagnetic fraction at room temperature is observed for shorter sintering time. Sintering tests are ongoing, and the results will be reported elsewhere.

This work also confirms that Mössbauer spectroscopy can be readily utilized to assess atomic-scale magnetism and the magnetic state of the materials, and in limited fashion, for the higher nickel content, the site occupancy of the Ni and Zn; more stringent determination for lower nickel content requires applied magnetic field measurements.

As witnessed by the decrease in hyperfine field at room temperature associated with lower magnetic ordering temperature with decreasing nickel content, the optimization of dopants in ferritic spinel compositions can be systematically evaluated for applications in magnetic wireless charging. Powder samples can be used to benchmark starting magnetic ordering before proceeding to more time intensive component fabrication and sintering steps. In future research, conversion X-ray Mössbauer spectroscopy will also be used to characterize final sintered magnetic components (in conversion x-ray reflection mode) to determine how atomic-scale magnetism has been impacted during the processing and densification steps.

In comparison with nickel-zinc ferrites prepared by other methods, we note that the low-temperature Mössbauer spectra feature rather narrow lines, very similar with those reported by

Leung et al. [13] for their materials prepared by solid state synthesis and refiring at 1200 ºC. In this context, fits with local environment distributions, as were utilized in Ref. [42] were not necessary. We also observe, see Figure 6 for x=0.5, as reported by Albuquerque et al. [43],that there is systematic narrowing of the lines with increasing heat treatment. Unsuprisingly, the hyperfine fields are somewhat larger and the linewidth are narrower than in nanostructured materials, *e.g.* 10-nm-sized $Ni_{0.2}Zn_{0.8}Fe_2O_4$ in Ref. [44], and 4-nm-sized $Ni_{0.5}Zn_{0.5}Fe_2O_4$ prepared by low-temperature self-combustion that was not followed by heat treatment.[39]

The color of the materials gives easy but limited information on the composition. Whereas pure zinc ferrite, CAS No.:68187-51-9, is classified as Pigment Yellow 119, a light tan/brown color, in contrast, nickel ferrite is darker with reported colors between dark brown and dark grey. The color evolution has been ascribed to change in an absorbance band near 700 nm wavelength, related to nickel in octahedral coordination that shifts to higher wavelength with increasing zinc content.[36] Whereas the color in a series of samples treated at ~1100-1300 ºC (0.2-0.9 in Fig. 3) exhibit very similar luminosity ($28.4 \leq L^* \leq 29.8$) and evolve systematically, the samples with $Ni_{0.5}Zn_{0.5}$ with lower temperature heat treatment exhibit more variation in L^* and significantly larger $a^*$and b^* values. We also note that the $NiFe_2O_4$ (NF) and $Ni_{0.5}Zn_{0.5}Fe_2O_4$ (NZF) nanopowders obtained by nitrate combustion and reported in Ref. [36] exhibit a similar trend of increasing a^* with Zn content, but larger b^* values, *i.e.* more yellow tinge. Detailed analysis of these variations is beyond the scope of this work, though appears that a more systematic investigation of the correlation between color, composition, microstructure, and heat treatment is warranted.

5. Conclusion

Nickel/zinc spinel ferrites prepared by a self-combustion reaction followed by heat treatment present XRD patterns indicating well crystallized materials. Likewise, the low-temperature Mössbauer spectra feature narrow lines and hyperfine fields and site occupation for the *A* and *B* sites in agreement with literature. Despite the absence of applied field data, a clear trend in hyperfine field with nickel composition is observed that could serve to estimate the Ni/Zn composition. A gradual, though not systematic, evolution of color is also observed with increasing nickel content. Overall, the presented combustion synthesis method offers facile tuneability in compositions, which combined with the possibility of rapid characterization of atomic local magnetism by Mössbauer spectroscopy enables advances in the compositional and processing space at a fast pace. This methodology can be easily transferred to similar spinel

ferrites. However, if more precise characterization of site occupancy or of spin-canting is required, Mössbauer spectral measurements in applied magnetic field are needed.

6. Acknowledgements

This research was sponsored by the Powertrain Materials Core Program, Department of Energy, Energy Efficiency and Renewable Energy, Vehicle Technologies Office. The authors would like to thank Steward Advanced Materials for the synthesis of the ferrite powders. The authors would also like to thank J. Allen Haynes and Jerry Gibbs for their program support and Gabriel Veith and Thomas Watkins for internal reviews.

Received: ((will be filled in by the editorial staff))
Revised: ((will be filled in by the editorial staff))
Published online: ((will be filled in by the editorial staff))

Nickel-zinc spinel ferrites prepared by self-combustion reaction followed by heat treatment present X-ray diffraction patterns indicative of well crystallized material, proving the tunability of this synthetic method. Low-temperature Mössbauer spectra exhibit narrow lines with a hyperfine fields and site occupation evolution for the *A* and *B* sites versus nickel content in agreement with those seen in solid-state reaction material.

R. P. Hermann*, G. Yumnam, K. D. Ardrey, and B. L. Armstrong

A Mössbauer spectroscopy investigation of nickel-zinc ferrites synthesized by self-combustion method for soft magnetic core application in wireless chargers

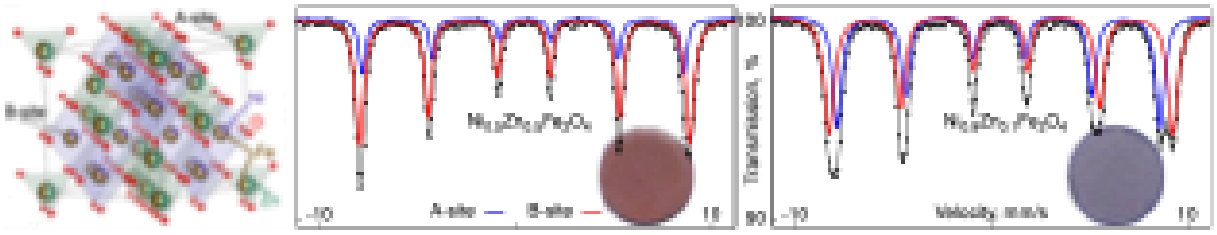

References

[1] K. Mohit, V. R. Gupta, N. Gupta, and S. K. Rout, Structural and microwave characterization of $Ni_{0.2}Co_xZn_{0.8-x}Fe_2O_4$ for antenna applications, *Ceram Int* **40**, 1575 (2014).

[2] A. Goldman, *Modern Ferrite Technology* (Springer, New York, NY, 2005), Second edn., p. 438.

[3] R. Valenzuela, Novel Applications of Ferrites, *Physics Research International* **2012**, 1 (2012).

[4] V. G. Harris, Modern Microwave Ferrites, *IEEE Transactions on Magnetics* **48**, 1075 (2012).

[5] E. Umut, M. Coskun, F. Pineider, D. Berti, and H. Gungunes, Nickel ferrite nanoparticles for simultaneous use in magnetic resonance imaging and magnetic fluid hyperthermia, *J Colloid Interface Sci* **550**, 199 (2019).

[6] A. B. Gadkari, T. J. Shinde, and P. N. Vasambekar, Ferrite Gas Sensors, *IEEE Sensors Journal* **11**, 849 (2011).

[7] M. Mohammad and S. Choi, in *2018 IEEE Applied Power Electronics Conference and Exposition (APEC)*2018).

[8] R. M. White, Opportunities in magnetic materials, *Science* **229**, 11 (1985).

[9] M. Sugimoto, The past, present, and future of ferrites, *J Am Ceram Soc* **82**, 269 (1999).

[10] H. Qin, Y. He, P. Xu, D. Huang, Z. Wang, H. Wang, Z. Wang, Y. Zhao, Q. Tian, and C. Wang, Spinel ferrites (MFe(2)O(4)): Synthesis, improvement and catalytic application in environment and energy field, *Adv Colloid Interface Sci* **294**, 102486 (2021).

[11] A. Goldman, in *Handbook of Modern Ferromagnetic Materials* (Springer US, Boston, MA, 1999), pp. 207.

[12] R. J. Joseyphus and J.-M. Greneche, in *Fundamentals of ^{57}Fe Mössbauer Spectrometry* (Springer Nature Singapore, Singapore, 2024), pp. 265.

[13] L. K. Leung, B. J. Evans, and A. H. Morrish, Low-Temperature Mössbauer Study of a Nickel-Zinc Ferrite:$ZnxNi_{1-x}Fe_2O_4$, *Phys. Rev. B* **8**, 29 (1973).

[14] R. S. Hargrove and W. Kündig, Mössbauer measurements of magnetite below the Verwey transition, *Solid State Commun* **8**, 303 (1970).

[15] L. Néel, Antiferromagnetism and Ferrimagnetism, *Proceedings of the Physical Society. Section A* **65**, 869 (1952).

[16] B. Pandey, F. Litterst, and E. Baggio-Saitovitch, Preferential spin canting in nanosize zinc ferrite, *J. Magn. Magn. Mater.* **385**, 412 (2015).

[17] D. Peddis, N. Yaacoub, M. Ferretti, A. Martinelli, G. Piccaluga, A. Musinu, C. Cannas, G. Navarra, J. M. Greneche, and D. Fiorani, Cationic distribution and spin canting in CoFe2O4 nanoparticles, *J Phys Condens Matter* **23**, 426004 (2011).

[18] D. Zagorac, H. Mueller, S. Ruehl, J. Zagorac, and S. Rehme, Recent developments in the Inorganic Crystal Structure Database: theoretical crystal structure data and related features, *J. Appl. Crystallogr.* **52**, 918 (2019).

[19] E. Wolska, W. Wolski, P. Piszora, M. Pietrusik, J. Subrt, T. Grygar, and M. Nejezchleba, X-ray powder diffraction and Mossbauer studies on the formation of $Cd_{0.5}Ni_{0.5}Fe_2O_4/Zn_{0.5}Ni_{0.5}Fe_2O_4$ spinel solid solutions, *Int J Inorg Mater* **1**, 187 (1999).

[20] K. Momma and F. Izumi, for three-dimensional visualization of crystal, volumetric and morphology data, *J. Appl. Crystallogr.* **44**, 1272 (2011).

[21] M. S. W. S. R. Lampman, T. B. Zorc,, *Engineered Materials Handbook* 1991), Vol. Volume 4: Ceramics and Glasses, ASM International.

[22] X. Lu, G. Liang, Q. Sun, and C. Yang, High-frequency magnetic properties of Ni-Zn ferrite nanoparticles synthesized by a low temperature chemical method, *Mater Lett* **65**, 674 (2011).
[23] P. Thakur, D. Chahar, S. Taneja, N. Bhalla, and A. Thakur, A review on MnZn ferrites: Synthesis, characterization and applications, *Ceram Int* **46**, 15740 (2020).
[24] K. D. Ardrey, R. D. McAuliffe, and B. L. Armstrong, The role of ferrites in wireless charging systems for electric vehicles, *J. Magn. Magn. Mater.* **610** (2024).
[25] T. Gaudisson, S. Nowak, Z. Nehme, N. Menguy, N. Yaacoub, J. M. Grenèche, and S. Ammar, Polyol-Made Spinel Ferrite Nanoparticles-Local Structure and Operating Conditions: $NiFe_2O_4$ as a Case Study, *Front Mater* **8** (2021).
[26] A. M. Kumar, K. H. Rao, and J. M. Greneche, Mossbauer investigation on Ni-Zn nanoferrite with the highest saturation magnetization, *J. Appl. Phys.* **105** (2009).
[27] S. K. Date, P. A. Joy, P. S. A. Kumar, B. Sahoo, and W. Keune, Structural, magnetic and Mossbauer studies on nickel-zinc ferrites synthesized via a precipitation route, *Second Seeheim Conference on Magnetism, Proceedings*, 3495 (2004).
[28] C. A. P. Gómez, C. A. B. Meneses, and A. Matute, Structural parameters and cation distributions in solid state synthesized Ni-Zn ferrites, *Mater Sci Eng B-Adv* **236**, 48 (2018).
[29] N. Chandamma, B. M. Manohara, B. S. Ujjinappa, G. J. Shankarmurthy, and M. V. S. Kumar, Structural and electrical properties of Zinc doped Nickel ferrites nanoparticles prepared via facile combustion technique, *J Alloy Compd* **702**, 479 (2017).
[30] S. Kumar, J. Singh, H. Kaur, H. Singh, and H. S. Dosanjh, Microstructural and magnetic properties of Zn substituted nickel ferrite synthesised by facile solution combustion method, *Micro Nano Lett* **14**, 727 (2019).
[31] V. Sreeja, S. Vijayanand, S. Deka, and P. A. Joy, Magnetic and Mossbauer spectroscopic studies of NiZn ferrite nanoparticles synthesized by a combustion method, *Hyperfine Interact* **183**, 99 (2008).
[32] H. Xue, Z. H. Li, X. X. Wang, and X. Z. Fu, Facile synthesis of nanocrystalline zinc ferrite via a self-propagating combustion method, *Mater Lett* **61**, 347 (2007).
[33] B. H. Toby and R. B. Von Dreele, GSAS-II : the genesis of a modern open-source all purpose crystallography software package, *J. Appl. Crystallogr.* **46**, 544 (2013).
[34] I. Levin, *NIST Inorganic Crystal Structure Database, NIST Standard Reference Database Number 3, National Institute of Standards and Technology, https://doi.org/10.18434/M32147 (Accessed 2025-01-29) (2018)*.
[35] CIE Standard in *Colorimetry-part 4: CIE 1976 L* a* b* colour space International Standard*(2007), pp. 2019.
[36] A. C. F. M. Costa, A. M. D. Leite, H. S. Ferreira, R. H. G. A. Kiminami, S. Cava, and L. Gama, Brown pigment of the nanopowder spinel ferrite prepared by combustion reaction, *J Eur Ceram Soc* **28**, 2033 (2008).
[37] L. Rebbouh, R. P. Hermann, F. Grandjean, T. Hyeon, K. An, A. Amato, and G. J. Long, Fe Mossbauer spectral and muon spin relaxation study of the magnetodynamics of monodispersed γ-Fe_2O_3 nanoparticles, *Phys. Rev. B* **76** (2007).
[38] V. Blanco-Gutiérrez, F. Jiménez-Villacorta, P. Bonville, M. J. Torralvo-Fernández, and R. Sáez-Puche, X-ray Absorption Spectroscopy and Mossbauer Spectroscopy Studies of Superparamagnetic $ZnFe_2O_4$ Nanoparticles, *J. Phys. Chem. C* **115**, 1627 (2011).
[39] V. D. Sudheesh, J. Nehra, A. Vinesh, V. Sebastian, N. Lakshmi, D. P. Dutta, V. R. Reddy, K. Venugopalan, and A. Gupta, Investigation of structural and magnetic properties of $Ni_{0.5}Zn_{0.5}Fe_2O_4$ nano powders prepared by self combustion method, *Mater Res Bull* **48**, 698 (2013).

[40] J. Chappert and R. B. Frankel, Mossbauer Study of Ferrimagnetic Ordering in Nickel Ferrite and Chromium-Substituted Nickel Ferrite, *Phys. Rev. Lett.* **19**, 570 (1967).
[41] C. A. Barrero, J. Arpe, E. Sileo, L. C. Sánchez, R. Zysler, and C. Saragovi, Ni- and Zn-doped hematite obtained by combustion of mixed metal oxinates, *Physica B* **354**, 27 (2004).
[42] C. A. P. Gómez, C. A. B. Meneses, and J. A. Jaén, Raman, infrared and Mossbauer spectroscopic studies of solid-state synthesized Ni-Zn ferrites, *J. Magn. Magn. Mater.* **505** (2020).
[43] A. S. Albuquerque, J. D. Ardisson, W. A. A. Macedo, and M. C. M. Alves, Nanosized powders of NiZn ferrite: Synthesis, structure, and magnetism, *J. Appl. Phys.* **87**, 4352 (2000).
[44] A. P. Kazin, M. N. Rumyantseva, V. E. Prusakov, I. P. Suzdalev, and A. M. Gaskov, Cation distribution in nanocrystalline $Ni_xZn_{1-x}Fe_2O_4$ spinel ferrites, *Inorg Mater+* **48**, 525 (2012).